Crump, Wayne; Välimaa, Alpo; Sillanpää, Mika A.

Coupling high-overtone bulk acoustic wave resonators via superconducting qubits

Published in:
Applied Physics Letters

DOI:
10.1063/5.0166924

Published: 25/09/2023

Document Version
Publisher's PDF, also known as Version of record

Please cite the original version:
Crump, W., Välimaa, A., & Sillanpää, M. A. (2023). Coupling high-overtone bulk acoustic wave resonators via superconducting qubits. *Applied Physics Letters*, *123*(13), 1-5. Article 134004. https://doi.org/10.1063/5.0166924

Applied Physics Letters

RESEARCH ARTICLE | SEPTEMBER 27 2023

Coupling high-overtone bulk acoustic wave resonators via superconducting qubits

Wayne Crump; Alpo Välimaa; Mika A. Sillanpää

Appl. Phys. Lett. 123, 134004 (2023)
https://doi.org/10.1063/5.0166924

Coupling high-overtone bulk acoustic wave resonators via superconducting qubits

Cite as: Appl. Phys. Lett. **123**, 134004 (2023); doi: 10.1063/5.0166924
Submitted: 8 July 2023 · Accepted: 14 September 2023 ·
Published Online: 27 September 2023

Wayne Crump, Alpo Välimaa, and Mika A. Sillanpää[a)]

AFFILIATIONS

Department of Applied Physics, Aalto University, P.O. Box 15100, FI-00076 Aalto, Finland

[a)]Author to whom correspondence should be addressed: Mika.Sillanpaa@aalto.fi

ABSTRACT

In this work, we present a device consisting of two coupled transmon qubits, each of which are coupled to an independent high-overtone bulk acoustic wave resonator (HBAR). Both HBAR resonators support a plethora of acoustic modes, which can couple to the qubit near resonantly. We first show qubit–qubit interaction in the multimode system and, finally, quantum state transfer where an excitation is swapped from an HBAR mode of one qubit to an HBAR mode of the other qubit.

Hybrid quantum systems seek to combine strengths and offset weaknesses of different quantum technologies in order to improve capability beyond that of any one technology. Superconducting circuits are one of the more mature quantum technologies at this stage and have been integrated with many other systems due to the relative ease in design and fabrication as well as good coherence times.[1]

Many different acoustic systems have been integrated with superconducting circuits such as nanomechanical oscillators,[2–6] phononic crystals,[7] bulk acoustic wave systems,[8,9] and surface acoustic wave systems.[10–15] Acoustic resonators can offer great coherence properties[16] as well as smaller mode volumes due to the relation between wave velocity and wavelength, with the difficulty coming in coupling these resonators strongly with electromagnetic systems.

The strong coupling of acoustic modes with superconducting qubits has resulted in many experiments exploring the quantum nature of mechanical oscillations, with experiments demonstrating number splitting,[7] the creation of non-classical states in the acoustic mode,[17] Landau–Zener–Stückelberg interference,[18,19] and entanglement.[20] The ability to prepare acoustic resonators in arbitrary quantum states opens up the possibility of using them in applications such as quantum memories due to their coherence properties and insensitivity to electromagnetic noise.

High-overtone bulk acoustic wave resonators (HBAR) offer access to mechanical modes in the GHz regime, making them attractive for integration with superconducting qubits. The piezoelectric interaction enables coupling in the strong regime and their state to be controlled and readout using the qubit. The system has been implemented using 3D[8] and 2D[9] transmon architectures with part or all of the qubit capacitor directly patterned on the piezo layer of the HBAR. This was later improved in both cases by using a flip-chip design,[17,21] which leads to the current state of the art.[22] Experiments on these system have demonstrated the creation of non-classical multiphonon states,[17] demonstration of dispersive readout for a parity measurement of the mechanical mode,[22] and sideband control of the mechanical modes.[21,23]

Work, thus, far has focused on coupling of a qubit and a single HBAR device, supporting a set of acoustic modes. In this work, we couple two complete qubit-HBAR systems together via qubit–qubit interaction and transfer excitations within the system,[24] including between the HBAR modes. This demonstrates the possibility of integrating multiple HBAR devices into quantum circuits, enabling the exploration of much larger and complex systems.

In the system, there are two qubits, which are coupled together as well as being individually coupled to a set of HBAR modes. The qubit-mode couplings can be described by the Jaynes–Cummings model, and the qubit–qubit coupling will be capacitive and therefore expected to take the iSWAP form.[25] The system as a whole can then be described by the Hamiltonian

$$
\begin{aligned}
H/\hbar = {} & \frac{\omega_1}{2}\sigma_{z,1} + \frac{\omega_2}{2}\sigma_{z,2} + J(\sigma_{+,1}\sigma_{-,2} + \sigma_{-,1}\sigma_{+,2}) \\
& + \sum_m \left[\omega_{m,1}\left(a^\dagger_{m,1}a_{m,1} + \frac{1}{2}\right) + g_{m,1}\left(a^\dagger_{m,1}\sigma_{-,1} + a_{m,1}\sigma_{+,1}\right)\right] \\
& + \sum_n \left[\omega_{n,2}\left(a^\dagger_{n,2}a_{n,2} + \frac{1}{2}\right) + g_{n,2}\left(a^\dagger_{n,2}\sigma_{-,2} + a_{n,2}\sigma_{+,2}\right)\right],
\end{aligned} \tag{1}
$$

where ω_1 and ω_2 are the qubit frequencies, J is the qubit–qubit coupling, $\omega_{m,1}$ and $\omega_{n,2}$ are the HBAR mode frequencies corresponding to their respective qubits, and $g_{m,1}$ and $g_{n,2}$ are the couplings to the HBAR modes. The $\sigma_{i,j}$ are the pauli operators, and a_m and $a_m^\dagger$ are the annihilation and creation operators, respectively.

In order to theoretically analyze the experiments described later, we determine the time evolution of the system using the Lindblad master equation. We include the qubits' decay and dephasing as well as mechanical mode decay.

Figure 1(a) shows an optical image of the device used for the experiments. The device consists of a superconducting circuit with two qubits, each with their own readout, flux bias control, and excitation lines. The qubits have a capacitive coupling to each other as well as to the HBAR flip chip that covers both. The qubits have a round pad on the bottom arm of around 80 μm in diameter, which defines the capacitive coupling to the HBAR chip through the capacitances C_1 and C_2 indicated in Fig. 1(b). The circuit was patterned using electron beam lithography and metalized with evaporated aluminum. Double angle evaporation was used to create the Josephson junctions for the qubits.

The HBAR flip chip [Fig. 1(b)] consists of a 900 nm AlN piezo layer, a 250 μm sapphire layer, and a 60 nm Mo layer in-between to act as a ground plane to enhance the coupling to the mechanical modes.[21] The vacuum gap on the order 4 μm for both qubits is estimated[26] based on the measured qubit-HBAR couplings mentioned later. The HBAR was placed by hand onto the circuit chip and glued with standard epoxy.

It is important to determine whether or not the qubits couple to the same set of acoustic modes. On the one hand, the qubits are in close proximity to each other and share the same HBAR chip, which would point to delocalized acoustic modes. On the other hand, the electric field of either qubit should confine the HBAR mode only below its own electrode. A finite-element simulation of a complete flip chip is beyond reach primarily due to the large overtone numbers. However, a simplified 3-dimensional geometry, where we used only 10 μm thick HBAR substrate, thus restricting the overtone number, and where also the qubit electrodes are positioned directly on the piezo surface, is computationally tractable. The simulation result shown in Fig. 1(c) indicates that the HBAR modes are strongly localized below either qubit's electrode, and, thus, we expect that each qubit will only couple to its own HBAR modes.

The qubit frequencies can be tuned in the range 3.7–4.5 GHz and have readout resonator frequencies of 6.230 and 6.013 GHz. The operating points of the qubits were chosen to maximize their coherence properties, and, hence, they are operating at or close to their minimum frequencies. Figure 2 shows two-tone measurements sweeping the qubit frequencies in the neighborhood of their operating frequencies chosen for later experiments. The operating frequency of qubit 1 was set near its minimum at $\omega_{1,\mathrm{OP}}/2\pi = 3.7778$ GHz and qubit 2 at its

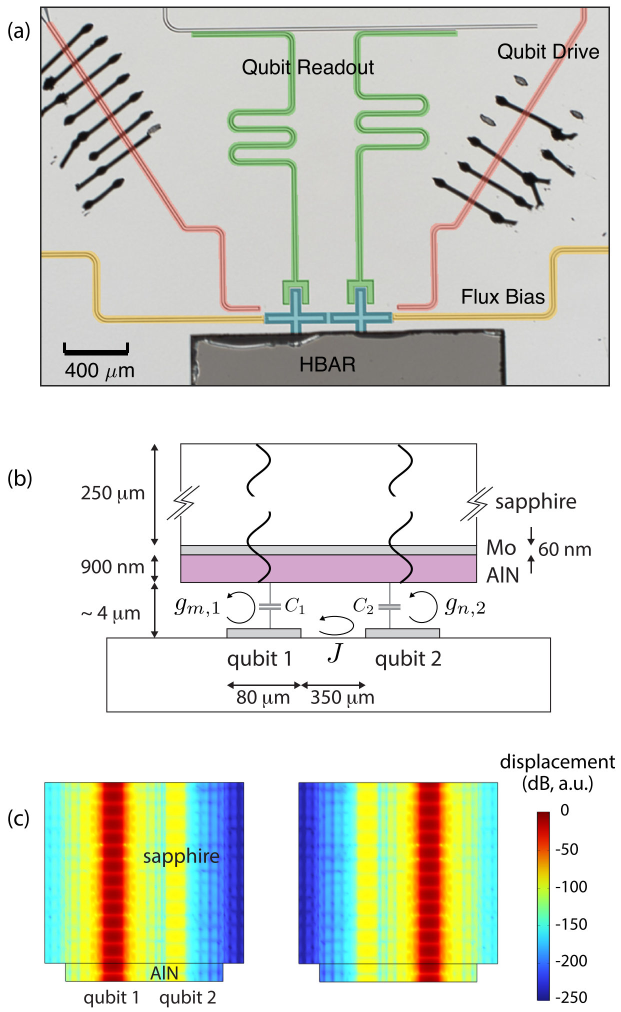

FIG. 1. Sample overview. (a) Optical image of the sample used in the experiment. It consists of two capacitively coupled qubits (blue) and an HBAR flip chip over the two qubits. Each qubit has separate control lines for flux (yellow), excitation (red), and a readout resonator (green). (b) Sideview schematics of the flip chip. The HBAR chip is on top. (c) Simplified finite-element simulation of HBAR modes at the qubit electrodes. A mode associated with qubit 1 is shown on the left, and similarly for qubit 2 on the right.

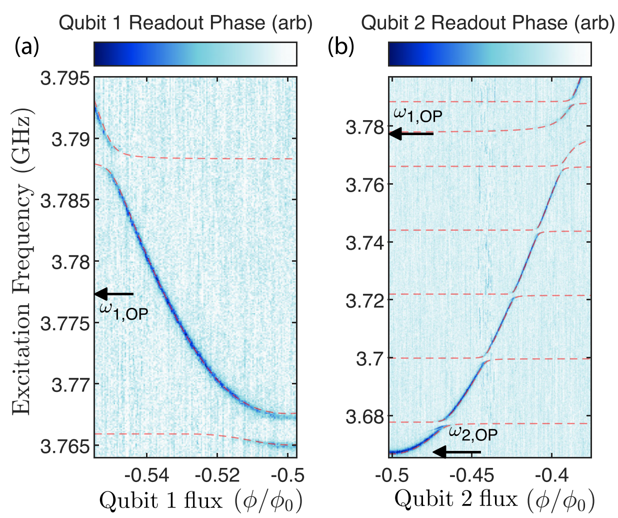

FIG. 2. Two-tone spectroscopy. (a) Qubit 1 around its operating point. (b) Qubit 2 around its operating point. In (a-b), the eigenvalues of Eq. (1) are plotted on top as dashed lines, and the operation points of the qubits in the transfer experiments are labeled.

minimum at $\omega_{2,\mathrm{OP}}/2\pi = 3.6673$ GHz. The many small anticrossings occur when a qubit is sweeping past an HBAR mode, while the larger anticrossing at 3.778 GHz seen in the data for qubit 2 corresponds to the qubit–qubit coupling. The spacing between HBAR modes (free spectral range, FSR) is around 22 MHz, which corresponds well with the thickness of the HBAR sapphire layer. The dashed lines in Fig. 2 show the eigenvalues according to Eq. (1).

At the qubits respective operating points, they had T_1 values of 2.2 and 2.41 μs as well as T_2 values of 4.41 and 1.02 μs. Their respective $2g$ couplings to their HBAR modes were 2.55 and 2.85 MHz, with the mechanical T_1 values being 380 and 320 ns. The system had a qubit–qubit $2g$ coupling of 16.7 MHz.

Figure 3 shows a vacuum Rabi oscillation experiment where an excitation is swapping between an initially excited qubit and its coupled mechanical modes. In panels (a) and (b), qubit 2 is being controlled and measured. At zero flux pulse amplitude, the qubit 2 frequency equals the operating frequency $\omega_{2,\mathrm{OP}}$ indicated in Fig. 2(b), while qubit 1 is parked at $\omega_{1,\mathrm{OP}}$. We see vacuum Rabi oscillations with the mechanical modes (red arrows) and also with the other qubit (blue arrows), corresponding with the anticrossings seen in Fig. 2(b). In Figs. 3(c) and 3(d), qubit 1 is controlled, with the flux pulse amplitude now indicating the frequency excursion from $\omega_{1,\mathrm{OP}}$, and qubit 2 is parked at $\omega_{2,\mathrm{OP}}$. Qubit 1 experiences vacuum Rabi oscillations with its coupled mechanical modes following the anticrossings seen in Fig. 2(a). Since the flux is tuned in the positive direction, it first sweeps on resonance with the lower mode at 3.767 GHz and then with the upper mode (3.788 GHz) seen in Fig. 2(a).

If one looks closely, the vacuum Rabi oscillation fringes can be seen to be asymmetric, especially in Fig. 3(a), and this results in deviations from the master equation simulation for later times. A part of the asymmetry can be explained being due to off-resonant interaction between the qubit and the nearest mode, which occurs before the flux pulse because of the finite length of the π pulse (50 ns). This would only account for some of the asymmetry for modes near the qubit, as this drops off as the detuning increases. We, thus, attribute most of the asymmetry to distortion of the rectangular flux pulse due to nonlinear dependence of the qubit frequency on flux voltage.[27] This is expected to be the most relevant around the sweet spot, primarily affecting qubit 2, which is consistent with the data.

The line cuts in Fig. 3(b) show a double oscillation feature that occurs when qubit 2 is near the qubit 1 frequency. This is because the excitation is experiencing Rabi oscillations with both the other qubit and the nearby acoustic modes at the same time but on different time scales, hence the multiple oscillating feature.

We now discuss the localization of the acoustic modes, namely, if they couple only to either qubit. Experimentally, the issue cannot immediately be resolved in spectroscopy, since the HBAR spectral lines seen in Fig. 2 are equal within measurement uncertainties, which, however, is expected based on the geometry. A time-domain experiment was done to confirm that the qubits couple to their individual sets of acoustic modes. This was done by swapping an excitation from qubit 1 to its acoustic mode at 3.788 GHz and then tuning it away while tuning the qubit 2 on resonance with this mode. The experiment found no response and so concluded that the qubits, indeed, couple to separate modes with any stray coupling being too weak to observe.

Finally, we demonstrate the swapping of an excitation through the degrees of freedom of the system. Figure 4 shows the pulse sequence and measured data. The excitation swaps from the 3.7885 GHz HBAR mode coupled to qubit 1 all the way to various HBAR modes coupled to qubit 2. The resulting measurement data are similar to Fig. 3(a) as the last part of the pulse sequence is similar to that experiment; however, this excitation has traveled from an acoustic

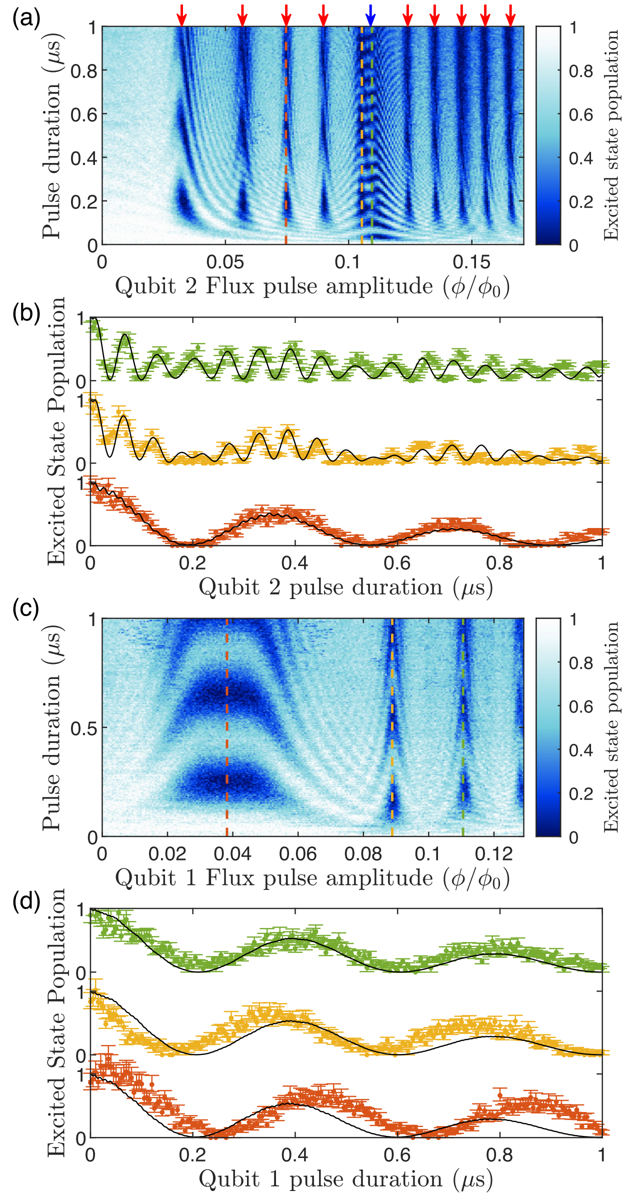

FIG. 3. Vacuum Rabi oscillations. (a) Qubit 2 is first excited, and then a square pulse of variable length and amplitude is applied to its flux control. Vacuum Rabi oscillations are seen between the right qubit and its coupled HBAR modes (red arrows) as well as with qubit 1 (blue arrows). (b) Line cuts along the dashed lines in (a), together with calculations using the Lindblad master equation and Eq. (1) (black lines). (c) The same experiment as before but using qubit 1. Now, we see vacuum Rabi oscillations between the qubit 1 and its coupled HBAR modes. (d) Line cuts along the dashed lines in (c), together with calculations using the Lindblad master equation and Eq. (1) (black lines).

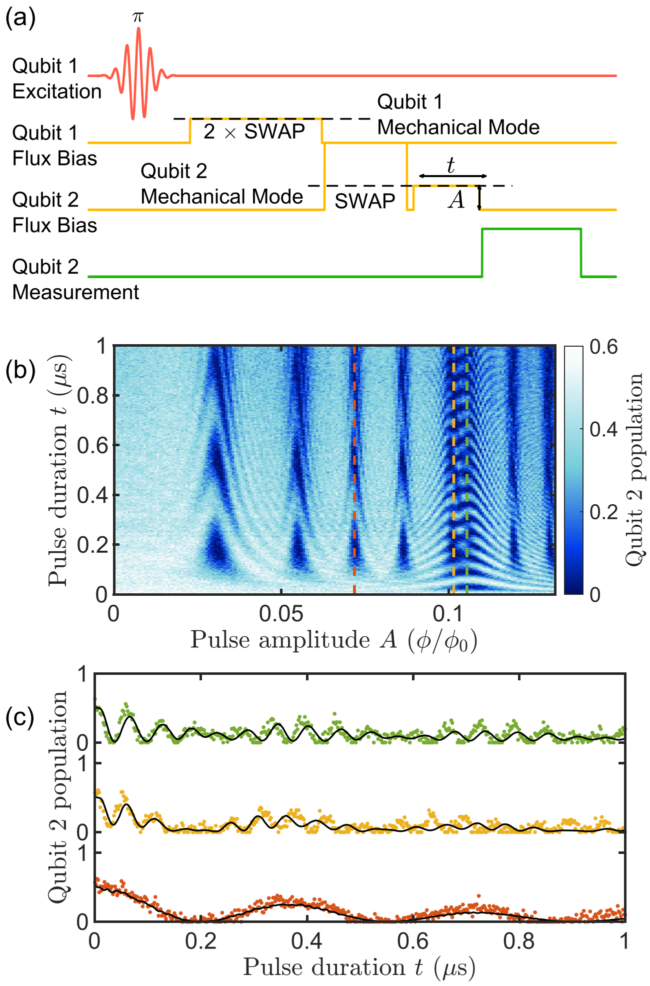

FIG. 4. Swapping an excitation throughout the system. (a) The pulse sequence for an experiment where an excitation is swapped between the degrees of freedom of the system. First, qubit 1 is excited with a π pulse; second, the excitation is swapped to a mechanical mode coupled to qubit 1 and back; third, the excitation is swapped to qubit 2; fourth, finally, a square pulse of variable amplitude and duration is applied to the qubit 2 flux bias, so we can see the excitation swapping to the mechanical modes coupled to qubit 2 as well as with qubit 1 again. (b) Experimental data using the pulse sequence shown at the top, where qubit 2 is measured after the pulse sequence. The data show Vacuum Rabi oscillations using an excitation that has traversed the system. (c) Line cuts as indicated by the dashed lines in (b) are plotted against the master equation solution.

mode coupled to the opposite qubit, which is why the initial excited state population is reduced due to decoherence.

Now that we have shown the ability to transfer excitations around the system, and we would, in principle, be able to create an entangled state between arbitrary acoustic modes. However, due to the limited coherence of the system, we were not able to measure this in practice. One needs to measure the entangled modes simultaneously under a series of tomography pulses in order to produce the density matrix of the system (for example, see Ref. 20). This was not straightforward to do in our system as the acoustic modes are coupled to different qubits, meaning we need to readout the acoustic mode in single-shot to be able to correlate the results. We are limited both by our single-shot readout fidelity <60% and by not being in the strong dispersive regime, which requires acoustic T_1 times of 8 μs at our coupling magnitudes.

A possible simplification to make is to only measure an entangled state, which does not occupy number states higher than $|1\rangle$, so that in this case, one can swap the state back to the qubits and measure them. Due to the low readout fidelity, we have to use an ensemble measurement. There is a tomography pulse scheme to measure the two qubit density matrix using an ensemble measurement.[28] This requires an appropriate two-qubit gate as a part of the tomography pulse scheme, and in our case, this would be an iSWAP pulse.

The calibration of this iSWAP pulse was problematic on two fronts. The first was that during the swap, around 45% of the excitation was lost, and the second was asymmetry, where in one direction, there was some residual excitation left in the initial qubit, while swapping in the other left no residual excitation. Part of the fidelity loss is caused by the qubit sweeping through many acoustic modes during the edges of the flux pulse. We carried out a simulation on this effect by a two-state restriction of the acoustic modes, obtaining a predicted 8% reduction of fidelity. Likely, some of the infidelity of the iSWAP is due to the qubit decoherence.

In order to improve the fidelity of single and two-qubit gates in the system, one would like the FSR to be larger than the coupling by a factor of at least 20. This is so that if the qubit is in between two modes, it will only interact dispersively. Also the FSR should be larger than inverse pulse widths, so that these are not exciting nearby mechanical modes as well. Longer coherence times for both the qubits and the acoustics are important toward this end. The ideal solution would be the development of a tunable coupler, to be able to selectively couple to modes of interest, which is important for using HBARs in quantum information processing.

In conclusion, we have fabricated and measured a sample consisting of two qubits each coupled to an individual set of high-overtone bulk acoustic (HBAR) modes as well as to each other. An excitation was swapped from an HBAR mode coupled with one qubit, to an HBAR mode coupled to the other qubit. This demonstrates the possibility to integrate multiple HBAR devices into a superconducting circuit, where complex quantum states could be stored across these devices.

We would like to thank Mikael Kervinen for useful discussion. We acknowledge the facilities and technical support of Otaniemi Research Infrastructure for Micro and Nanotechnologies (OtaNano) that is part of the European Microkelvin Platform. This work was supported by the Academy of Finland (Contract No. 352189), the European Research Council (No. 101019712), and the Wihuri Foundation. We acknowledge funding from the European Union's Horizon 2020 Research and Innovation Program under the QuantERA II Programme (No. 13352189). This work was performed as part of the Academy of Finland Centre of Excellence Program (Project No. 352932).

AUTHOR DECLARATIONS

Conflict of Interest

The authors have no conflicts to disclose.

Author Contributions

Wayne Crump: Formal analysis (lead); Investigation (lead). **Alpo Välimaa:** Methodology (equal). **Mika Sillanpaa:** Supervision (lead).

DATA AVAILABILITY

The data that support the findings of this study are available from the corresponding author upon reasonable request.

REFERENCES

[1] A. A. Clerk, K. W. Lehnert, P. Bertet, J. R. Petta, and Y. Nakamura, "Hybrid quantum systems with circuit quantum electrodynamics," Nat. Phys. **16**, 257–267 (2020).

[2] C. A. Regal, J. D. Teufel, and K. W. Lehnert, "Measuring nanomechanical motion with a microwave cavity interferometer," Nat. Phys. **4**, 555–560 (2008).

[3] J. D. Teufel, D. Li, M. S. Allman, K. Cicak, A. J. Sirois, J. D. Whittaker, and R. W. Simmonds, "Circuit cavity electromechanics in the strong-coupling regime," Nature **471**, 204–208 (2011).

[4] A. D. O'Connell, M. Hofheinz, M. Ansmann, R. C. Bialczak, M. Lenander, E. Lucero, M. Neeley, D. Sank, H. Wang, M. Weides, J. Wenner, J. M. Martinis, and A. N. Cleland, "Quantum ground state and single-phonon control of a mechanical resonator," Nature **464**, 697–703 (2010).

[5] L. Mercier de Lépinay, C. F. Ockeloen-Korppi, M. J. Woolley, and M. A. Sillanpää, "Quantum mechanics-free subsystem with mechanical oscillators," Science **372**, 625–629 (2021).

[6] S. Kotler, G. A. Peterson, E. Shojaee, F. Lecocq, K. Cicak, A. Kwiatkowski, S. Geller, S. Glancy, E. Knill, R. W. Simmonds, J. Aumentado, and J. D. Teufel, "Direct observation of deterministic macroscopic entanglement," Science **372**, 622–625 (2021).

[7] P. Arrangoiz-Arriola, E. A. Wollack, Z. Wang, M. Pechal, W. Jiang, T. P. McKenna, J. D. Witmer, R. Van Laer, and A. H. Safavi-Naeini, "Resolving the energy levels of a nanomechanical oscillator," Nature **571**, 537–540 (2019).

[8] Y. Chu, P. Kharel, W. H. Renninger, L. D. Burkhart, L. Frunzio, P. T. Rakich, and R. J. Schoelkopf, "Quantum acoustics with superconducting qubits," Science **358**, 199–202 (2017).

[9] M. Kervinen, I. Rissanen, and M. Sillanpää, "Interfacing planar superconducting qubits with high overtone bulk acoustic phonons," Phys. Rev. B **97**, 205443 (2018).

[10] M. V. Gustafsson, T. Aref, A. F. Kockum, M. K. Ekström, G. Johansson, and P. Delsing, "Propagating phonons coupled to an artificial atom," Science **346**, 207–211 (2014).

[11] A. Noguchi, R. Yamazaki, Y. Tabuchi, and Y. Nakamura, "Qubit-assisted transduction for a detection of surface acoustic waves near the quantum limit," Phys. Rev. Lett. **119**, 180505 (2017).

[12] R. Manenti, A. F. Kockum, A. Patterson, T. Behrle, J. Rahamim, G. Tancredi, F. Nori, and P. J. Leek, "Circuit quantum acoustodynamics with surface acoustic waves," Nat. Commun. **8**, 975 (2017).

[13] B. A. Moores, L. R. Sletten, J. J. Viennot, and K. W. Lehnert, "Cavity quantum acoustic device in the multimode strong coupling regime," Phys. Rev. Lett. **120**, 227701 (2018).

[14] A. Bienfait, K. J. Satzinger, Y. P. Zhong, H.-S. Chang, M.-H. Chou, C. R. Conner, É. Dumur, J. Grebel, G. A. Peairs, R. G. Povey, and A. N. Cleland, "Phonon-mediated quantum state transfer and remote qubit entanglement," Science **364**, 368–371 (2019).

[15] J. M. Kitzman, J. R. Lane, C. Undershute, P. M. Harrington, N. R. Beysengulov, C. A. Mikolas, K. W. Murch, and J. Pollanen, "Phononic bath engineering of a superconducting qubit," Nat. Commun. **14**, 3910 (2023).

[16] V. J. Gokhale, B. P. Downey, D. S. Katzer, N. Nepal, A. C. Lang, R. M. Stroud, and D. J. Meyer, "Epitaxial bulk acoustic wave resonators as highly coherent multi-phonon sources for quantum acoustodynamics," Nat. Commun. **11**, 2314 (2020).

[17] Y. Chu, P. Kharel, T. Yoon, L. Frunzio, P. T. Rakich, and R. J. Schoelkopf, "Creation and control of multi-phonon Fock states in a bulk acoustic-wave resonator," Nature **563**, 666–670 (2018).

[18] M. D. LaHaye, J. Suh, P. M. Echternach, K. C. Schwab, and M. L. Roukes, "Nanomechanical measurements of a superconducting qubit," Nature **459**, 960–964 (2009).

[19] M. Kervinen, J. E. Ramírez-Muñoz, A. Välimaa, and M. A. Sillanpää, "Landau-Zener-Stückelberg interference in a multimode electromechanical system in the quantum regime," Phys. Rev. Lett. **123**, 240401 (2019).

[20] E. A. Wollack, A. Y. Cleland, R. G. Gruenke, Z. Wang, P. Arrangoiz-Arriola, and A. H. Safavi-Naeini, "Quantum state preparation and tomography of entangled mechanical resonators," Nature **604**, 463–467 (2022).

[21] M. Kervinen, A. Välimaa, J. E. Ramírez-Muñoz, and M. A. Sillanpää, "Sideband control of a multimode quantum bulk acoustic system," Phys. Rev. Appl. **14**, 054023 (2020).

[22] U. von Lüpke, Y. Yang, M. Bild, L. Michaud, M. Fadel, and Y. Chu, "Parity measurement in the strong dispersive regime of circuit quantum acoustodynamics," Nat. Phys. **18**, 794–799 (2022).

[23] U. von Lüpke, I. C. Rodrigues, Y. Yang, M. Fadel, and Y. Chu, "Engineering phonon-phonon interactions in multimode circuit quantum acousto-dynamics," arXiv:2303.00730 (2023).

[24] M. A. Sillanpää, J. I. Park, and R. W. Simmonds, "Coherent quantum state storage and transfer between two phase qubits via a resonant cavity," Nature **449**, 438 (2007).

[25] S. Kwon, A. Tomonaga, G. Lakshmi Bhai, S. J. Devitt, and J.-S. Tsai, "Gate-based superconducting quantum computing," J. Appl. Phys. **129**, 041102 (2021).

[26] A. Välimaa, "Piezoelectric resonators in the quantum regime," Ph.D. thesis (Aalto University, 2022).

[27] M. A. Rol, L. Ciorciaro, F. K. Malinowski, B. M. Tarasinski, R. E. Sagastizabal, C. C. Bultink, Y. Salathe, N. Haandbaek, J. Sedivy, and L. DiCarlo, "Time-domain characterization and correction of on-chip distortion of control pulses in a quantum processor," Appl. Phys. Lett. **116**, 054001 (2020).

[28] M. Li, G. Xue, X. Tan, Q. Liu, K. Dai, K. Zhang, H. Yu, and Y. Yu, "Two-qubit state tomography with ensemble average in coupled superconducting qubits," Appl. Phys. Lett. **110**, 132602 (2017).